

In situ measurement of the internal stress evolution during sputter deposition of ZnO:Al

S. Michotte*, J. Proost

Institute of Mechanics, Materials and Civil Engineering, Universite catholique de Louvain, Place Sainte-Barbe 2, B-1348 Louvain-la-Neuve, Belgium

ARTICLE INFO

Article history:

Received 17 June 2011

Accepted 8 November 2011

Available online 30 November 2011

Keywords:

Transparent conductive oxides

In situ stress

Electro-optical properties

Strain engineering

ABSTRACT

Transparent and conductive ZnO:Al films were deposited by RF magnetron sputtering on opaque (Si/SiO₂) or transparent (glass) substrates. The internal stress evolution has been measured in situ using a high resolution 2D curvature measurement technique. Internal tensile or compressive stresses were generated, depending on the sputtering pressure, oxygen addition level and substrate temperature. The origin of the observed stress level is correlated with factors affecting the film growth mechanism, and the relation with the electro-optical properties of the resulting transparent and conductive oxide films is highlighted.

© 2011 Elsevier B.V. All rights reserved.

1. Introduction

Magnetron sputtered ZnO films are used in a variety of thin film applications. For example, ZnO films are extensively used in low-emissivity glasses [1] and are also the standard front transparent conducting oxide (TCO) contact in CIS [2] as well as silicon thin film solar cells [3,4]. Due to the limited resources of indium, ZnO:Al is an ideal replacement for ITO (Indium Tin Oxide) in many large scale applications. Indeed, ZnO:Al is only composed of elements that are non-toxic and abundant. The use of only abundant elements is crucial for solar cells, whose deployment at tera watt peak scale is generally limited by natural resource availability.

Strain engineering is an appealing way to improve the functional properties of these TCO layers (see Refs. [5–7] for reviews on stress in sputtered films). In this respect, it has already been observed that DC and MF sputtered ZnO:Al films with the lowest resistivity generally also had the lowest level of structural strain [8,9], the latter being determined from XRD diffractograms on as-deposited samples. Other reports have suggested a direct link between the crystal quality of RF sputtered ZnO, in terms of film texture and stoichiometry, and the level of internal compressive stress derived ex situ from peak shifts in micro-Raman spectra [10]. While the majority of the characterizations reported in the literature on the internal stress level in TCO films are still based on ex situ measurements in as-deposited samples, it is clear that efforts to further unravel the link between the internal stress and the resulting electro-optical properties would benefit largely from

in situ measurements of the internal stress evolution taken in real-time during the deposition process itself. Experimentally, this is also the most direct way to reveal the effect of the most critical deposition parameters. In this paper, we report on such in situ measurements of the internal stress evolution during RF sputtering of ZnO:Al thin films onto either Si/SiO₂ opaque substrates or transparent glass substrates by using a high resolution 2D curvature measurement technique. We will also highlight the dependence of those internal stresses on various sputter process parameters, as well as their relation with the electro-optical properties of the resulting layers.

2. Experiment

For the experiments, a turbopumped AJA deposition chamber with five 2 in magnetron guns (sputter up configuration) and a loadlock was used. The Ar and O₂ flow were regulated by mass flow controllers. The total sputtering pressure was measured by a capacitance vacuum meter (Baratron) and kept constant with a VAT valve controller. The deposition parameters are summarized in Table 1. Our deposition chamber is depicted in Fig. 1. The problematic bombardment of negative oxygen ions that has been reported to possibly lead to a spatial dependence of the deposit [11,12] is in our case minimized thanks to the relatively large target to substrate distance, combined with the rotation of the substrate and the delivery of the oxygen gas through small holes disposed along a ring directly at the level of the substrate. Furthermore, such oxygen ion bombardment issues are usually more pronounced in DC where the cathode voltage is much larger than in the present RF case (our cathode voltage amounts only to about 100 V).

* Corresponding author. Tel.: +32 1047 2484; fax: +32 1047 4028.
E-mail address: sebastien.michotte@uclouvain.be (S. Michotte).

Table 1
Deposition parameters.

Target-to-substrate distance	122 mm
Target diameter/thickness	54 mm/3 mm
Magnetic flux parallel to the target surface	0.4 T
Target purity	99.99% (Al ₂ O ₃ :ZnO 2 wt %)
Base pressure	3 × 10 ⁻⁶ Pa
Working pressure	1.5–10 mTorr (=0.2–1.33 Pa)
Ar+O ₂ flow rate	30 sccm (= 5 × 10 ⁻⁷ m ³ /s)
Effective pumping speed	700 l/s
Substrate potential	Floating
Substrate temperature	60 °C (not intentionally heated)–350 °C
Gas purity	Ar (> 99.9999%)/O ₂ (> 99.9995%)
Substrate rotation	40 rpm
Gun power	55 W
RF frequency	13.56 MHz
Chamber impedance	(2–18i) to (1.6–40i) (typically)

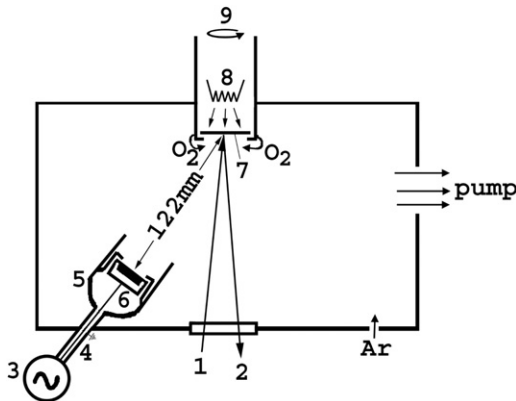


Fig. 1. Schematic of our deposition chamber: 1. incoming MOSS laser beams, 2. reflected laser beams, 3. RF generator + matching network, 4. coax cable, 5. one out of five confocal magnetron guns, 6. target, 7. substrate, 8. heater, 9. rotation. The position of the pump as well as the location of argon and oxygen gas is also depicted.

The ZnO target contained 2 wt % Al₂O₃ and was subjected to RF excitation. The films have been deposited onto 3 in wafers or 1 in by 1 in squares made of Si wafer 380 μm thick thermally oxidized (by LPCVD wet oxidation at 1000 °C) to give a SiO₂ layer of 540 nm on one hand or onto 1 in by 1 in extra clear selected float glasses (low iron content) 400 μm thick on the other hand. After transfer into the ultra-high vacuum chamber, the substrates were pre-cleaned with an RF-bias for a few minutes during which Ar atoms accelerated at 150 eV remove about 3–5 nm of the substrate.

There exist many ways to measure the internal stress, such as from the shift of XRD peaks [12] or from the bending of a cantilever or of an unconstrained wafer [13,14]. The latter, based on the so-called Multibeam Optical Stress Sensor (MOSS) proved to be very efficient for in situ internal stress monitoring in case of metal evaporation [13] or CVD and epitaxial films [14]. We therefore used the same MOSS-technique (from K-space) on our sputtering chamber to derive the internal stress evolution in real time. The combination of parallel beam illumination and CCD detection results in a system that is capable of measuring a radius of curvature as large as 10 km. In order to suppress the light from the plasma discharge, a bandpass filter (660 nm ± 4 nm) was mounted in front of the CCD. During deposition, a change in curvature Δκ is thus measured with a laser deflectometer as shown in Fig. 2a, which illuminates the sample with an array of 12 parallel laser beams, whose position and intensity is acquired by the CCD camera (Fig. 2b). Since the substrate was rotated for

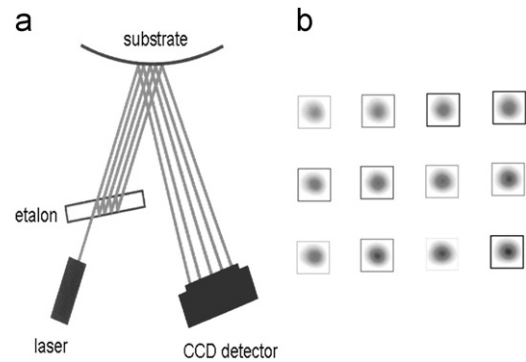


Fig. 2. (a) MOSS setup for measuring substrate curvature in real time. (b) Three by four spot array seen by the CCD camera.

better deposit uniformity, the CCD was triggered with a proximity sensor at every rotation. A frame grabber then records in real time the centroid position of each spot (the equivalent of their gravity center). According to Eq. (1)

$$\Delta\kappa = \frac{d-d_0^*}{d_0^*} \cdot G \quad (1)$$

the curvature change in the two in-plane directions of the deposited film is simply given by the mean differential spacing (where d_0^* is the spots spacing when the substrate is replaced by a perfectly flat mirror) times the optical distance G ($=0.68$ m here, as determined with a set of calibrated curved mirrors). The curvature change measured along the two in-plane directions of the film is then directly proportional to the product of the film mean internal stress $\langle\sigma_f\rangle$ and the film thickness h_f

$$\frac{Y_s \cdot h_s^2}{6} \cdot \Delta\kappa = \langle\sigma_f\rangle \cdot h_f = \int_0^{h_f} \sigma_{inst} \cdot dh_f \quad (2)$$

where Y_s is the biaxial modulus of the substrate and h_s is the substrate thickness. The substrate biaxial modulus may be expressed in terms of the Young Modulus E and the Poisson coefficient ν , such as $Y_s = E/(1-\nu)$ and amounts to 182 GPa or 92 GPa for a silicon or glass substrate, respectively. Since the deposited film is much thinner than the substrate, one advantage of this technique is that there is no need to know the modulus of the deposited film itself. Variations in film thickness were also measured in situ by a quartz crystal microbalance, and converted to absolute values based on the final film thickness measured ex-situ with cross-sectional SEM. The measured stress · thickness product can therefore be plotted versus the thickness inferred independently and the slope of a line connecting the origin to each point of such a curve represents the evolution of the film mean internal stress $\langle\sigma_f\rangle$ during the growth (i.e. the internal stress averaged through the film thickness). As can be seen in Eq. (2), the local slope can also be derived to obtain the evolution of the so-called instantaneous internal stress σ_{inst} , associated both with growth of new film, and relaxation occurring within the existing film. Note that positive values of stress · thickness imply a tensile mean stress, while negative values imply a compressive mean stress. Positive (negative) slopes correspond to a tensile (compressive) instantaneous stress.

Samples were also characterized ex situ after deposition. The substrate and film thickness was checked by cross-sectional SEM after each deposition. The phase structure was determined by X-ray diffraction, measured with Cu K α radiation in the usual $\theta-2\theta$ geometry. The sheet resistance at room temperature has been determined by a four-point probe. Optical transmission was measured with a spectrophotometer ranging from 300 to 850 nm with a 0.5 nm resolution.

3. Results and discussion

The impact of the main deposition parameters on the internal stress evolution of 400 nm thick ZnO:Al films, RF sputter deposited on either Si/SiO₂ or glass substrates, will be presented first. Notice that the surface of those two substrates types is amorphous. A comparison between Si/SiO₂ and glass substrates will then be given for the most relevant deposition parameter values in terms of the electro-optical functional properties. For all the conditions investigated, the resulting ZnO:Al films always presented a wurtzite structure with a nearly 100% texturization corresponding to the *c*-axis perpendicular to the substrate. Indeed, all the X-ray diffraction patterns presented a single peak at $2\theta = 34.5^\circ$ corresponding to the 002 direction of the ZnO lattice, as generally reported for ZnO:Al sputtered films [15]. The curvature measured in two perpendicular in-plane directions always gave identical results, so only one (with the lowest noise) is reported here. This corresponds well to a biaxial stress situation where $\sigma_{XX} = \sigma_{YY}$.

3.1. Influence of deposition parameters on the internal stress evolution

The three main deposition parameters that were varied, namely the working pressure, the oxygen gas addition level and the substrate temperature, present all a very strong and direct influence on the internal stress of the growing layer. Fig. 3 depicts the influence of the Ar working pressure on the internal stress evolution. The baseline level was checked to be constant with a zero mean value for at least ten minutes before the deposition, as can be seen in Fig. 3a. The deposit then starts at time zero and its end is indicated with a vertical arrow. The corresponding mean internal stress can be seen in Fig. 3b. As the Ar working pressure is varied from low to high pressure, the internal stress is seen to vary from compressive to tensile. Note that, to the best of our knowledge, only compressive stress levels have been reported so far for sputtered ZnO:Al layers [16,17,12]. As ZnO exhibits a high melting point ($T_m = 1975^\circ\text{C}$), this reported behavior is very similar to the one observed with the

sputtering of refractory metals such as Pd or Mo [18] where surface diffusion is relatively low. Indeed, by increasing the working pressure, adatoms suffer more collisions in the plasma such that their energies once they reach the growing surface can be reduced from initially a few tens of eV to only a few eV after many collisions. This can then in turn be related to the structure zone model within the Thornton diagram [19]. In this framework, zone 1 morphologies correspond to little adatom diffusion. It occurs at high working pressure (3 and 6 mTorr) with consequently low impact energies, resulting in a film which is not fully densified and tensile internal stress due to grain “zipping” [13]. Increasing the pressure further to 10 mTorr will just lead to an increase in the porosity. As the working pressure is reduced, adatoms impact the surface with a higher energy, and the morphology corresponds to the Thornton transitional zone with a more fibrous and compacted structure. The internal stress is then compressive, since adatoms become more susceptible to diffuse along grain boundaries and also because of atomic peening. We note that the grain size as determined by plane view SEM observations at a thickness of 400 nm ranges between 25 and 30 nm, independently of the working pressure. In the following, we choose 2 mTorr as the optimal working pressure, which is sufficiently low to ensure a good compact structure (columnar growth) but still high enough to avoid structural damage occurring when adatoms possess a too high incoming energy.

Fig. 4 shows the influence of oxygen addition on the internal stress evolution in the growing layer. At 2 mTorr, the stress is mainly compressive at low and high oxygen additions because of the predominance of atomic peening. The behavior when 0.2 sccm and 1 sccm O₂ is added is however drastically different and deserves consideration. Indeed, in terms of optical properties, it will be shown in Section 3.3 that the value of 0.2 sccm oxygen addition corresponds to the optimum parameter. To understand the growth mechanism, a Volmer–Weber growth mode is most probably occurring since adatom–adatom interactions are stronger than those of the adatom with the surface. This then leads to the formation of three-dimensional adatom clusters or islands [20]. The delayed tensile stress in the reported evolution at 0.2 sccm O₂ is related to the delayed percolation. A typical SEM

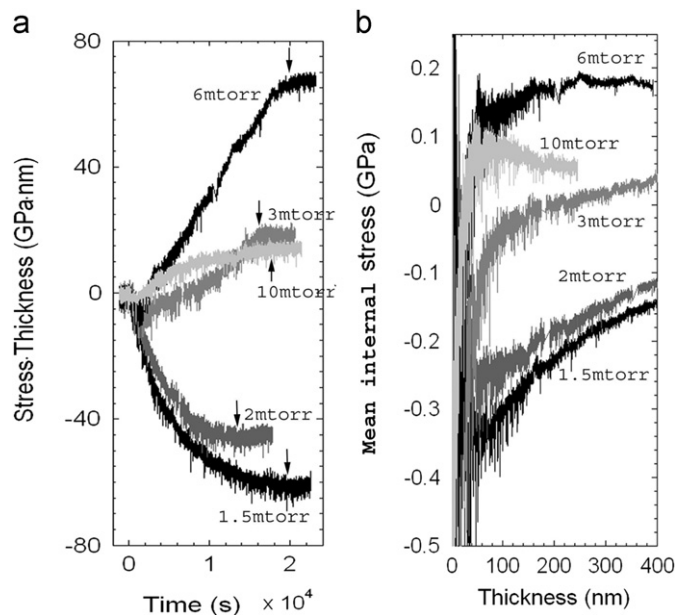


Fig. 3. Internal stress evolution for different ZnO:Al films grown on unheated Si/SiO₂ substrates with various argon pressures (without oxygen gas addition): (a) stress · thickness vs time (the deposit starts at time zero and its end is indicated by a vertical arrow), (b) mean internal stress vs thickness.

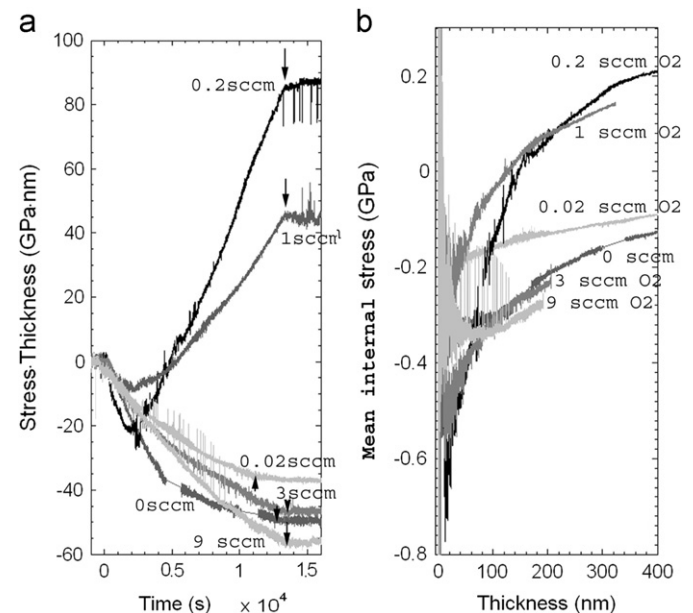


Fig. 4. Internal stress evolution for different ZnO:Al films grown on unheated glass substrates at a working pressure of 2 mTorr with a fixed argon flow of 30 sccm and various oxygen gas flows: (a) stress · thickness vs time (the deposit starts at time zero and its end is indicated by a vertical arrow), (b) mean internal stress vs thickness.

micrograph of the cross-section is shown in Fig. 5 for the ZnO:Al film grown at 2 mTorr on unheated glass with a 0.2 sccm oxygen flow. The typical columnar structure can easily be recognized. The grain percolation can also be identified and seems to occur for that condition at a thickness of about 75 nm. During grain percolation, it is well-established that interatomic forces try to close the gap at the grain boundaries by the so-called zipping mechanism [13], leading to a tensile instantaneous stress. The grain size is then further preserved because the insufficient homologous temperature (T/T_m) does not allow for grain growth or recrystallization. This then leads to further columnar growth. As can be seen in Fig. 6, where the stress · thickness product is plotted vs the thickness for 0.2 sccm oxygen, the percolation thickness can also be inferred from the internal stress evolution and indeed amounts to about 75 nm, where tensile instantaneous stress starts to appear.

Fig. 7 shows the influence of the substrate temperature on the internal stress evolution in the growing layer (without oxygen addition). A moderate heating to 150 °C is seen to be beneficial for

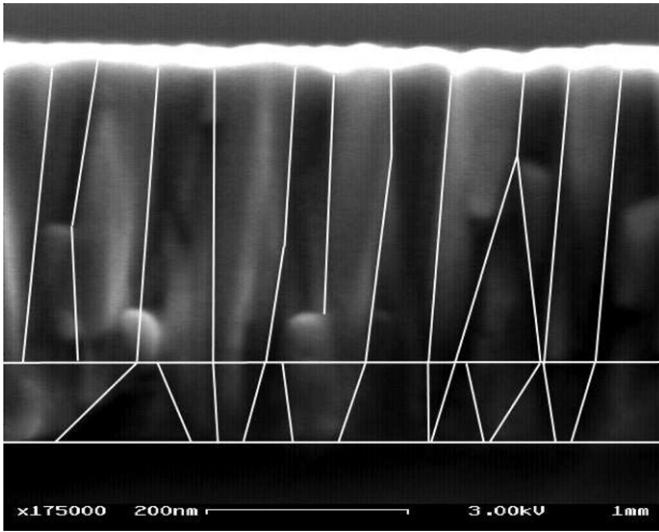


Fig. 5. Scanning electron micrograph of a 400 nm thick ZnO:Al film grown at 2 mTorr on unheated glass with a 0.2 sccm oxygen flow. The white straight lines have been added at some grain boundaries as guide for the eyes to illustrate the grain coalescence occurring at a thickness of about 75 nm, followed by columnar grain growth.

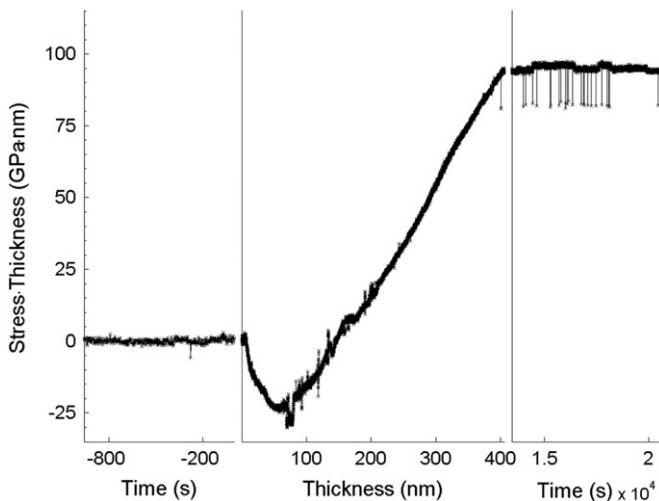


Fig. 6. Internal stress evolution for an ZnO:Al film grown on unheated glass substrates at a working pressure of 2 mTorr with fixed argon (30 sccm) and oxygen (0.02 sccm) gas flows: stress · thickness vs thickness.

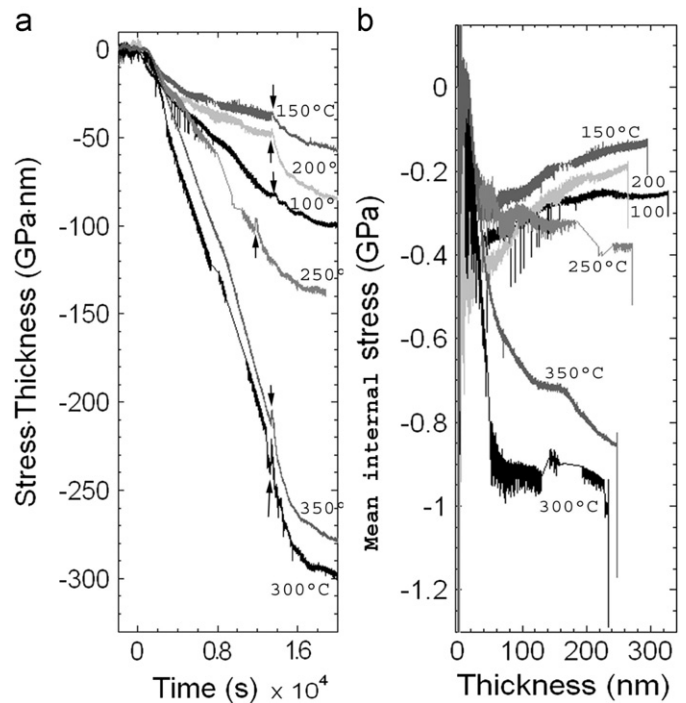


Fig. 7. Internal stress evolution for different ZnO:Al films grown on glass substrates at a working pressure of 2 mTorr (without oxygen gas addition) and various substrate temperatures: (a) stress · thickness vs time (the deposit starts at time zero and its end is indicated by a vertical arrow), (b) mean internal stress vs thickness.

reducing the compressive stress level. This temperature of 150 °C will be shown in Section 3.3 to correspond also to the one leading to the best electro-optical properties for the present deposition rate (0.3 Å/s). Increasing the substrate temperature corresponds to a displacement in the Thornton zone model at fixed Ar pressure toward increasing homologous temperature (T/T_m). The film structure then moves within the transitional zone toward zone 2, the latter corresponding to surface diffusion controlled growth. Therefore, as the substrate temperature becomes larger, more adatoms can diffuse along the grain boundaries, which has been shown to increase in turn the resulting compressive stress [21,22].

3.2. Influence of glass vs. oxidised silicon substrate on the internal stress evolution

As can be seen in Fig. 8 for the case of unheated substrates with or without the addition of oxygen, there is almost no dependence of the internal stress evolution in the ZnO:Al layer on the substrate nature. Since there is no heating in this case, no stress modulation occurs at the end of the deposition so that both the curvature as well as the stress retain their value at the end of the deposition. For depositions with substrate heating, the situation is however quite different as shown in Fig. 9. Although the growth-induced stress is again independent on the substrate type, the thermal stress that occurs after deposition upon cooling is either compressive for glass substrates or tensile for Si/SiO₂ substrates. This thermal stress is indeed related to the difference in linear thermal coefficient between ZnO:Al and the substrate. Since $\alpha_{\text{glass}} = 8.7 \times 10^{-6}/\text{K}$ is larger than $\alpha_{\text{ZnO}} = (1.784 + 0.0104 T) \times 10^{-6}/\text{K}$, with T expressed in kelvin and ranging from 300 to 650 K, glass tends to contract more upon cooling than the ZnO:Al layer. This therefore induces a compressive thermal stress in the ZnO:Al layer. Note that this additional post-deposition compressive stress component was already evidenced in Fig. 7, the magnitude of which scaling

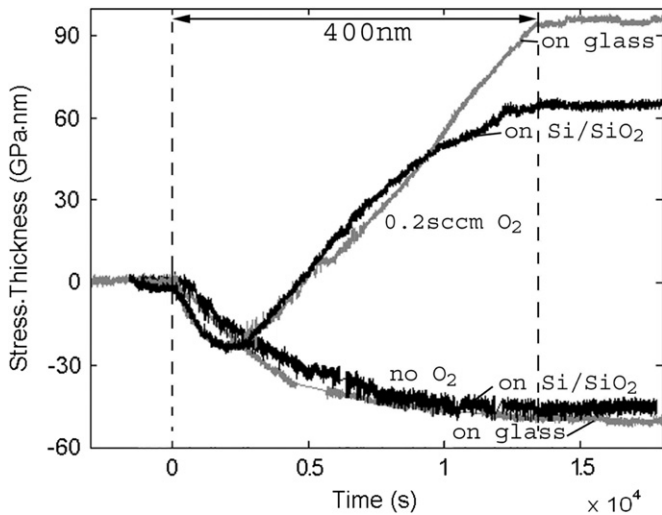


Fig. 8. Stress · thickness vs time evolution during the deposition of 400 nm ZnO:Al at 2 mTorr without intentional heating. Comparison between Si/SiO₂ and glass substrates for either no oxygen gas addition or a 0.2 sccm flow of oxygen.

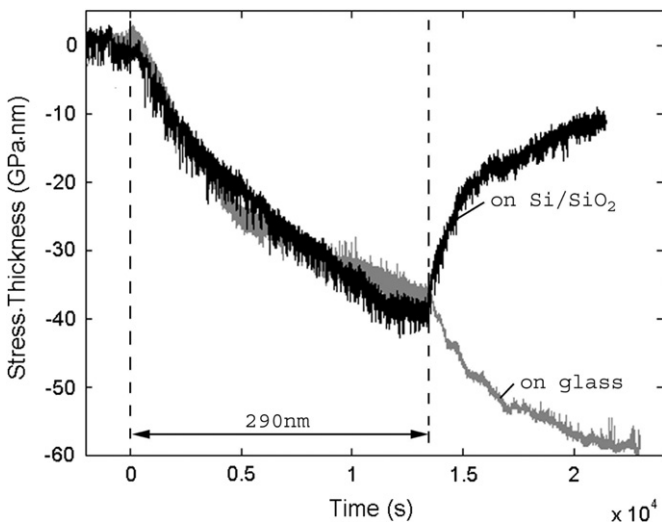


Fig. 9. Stress · thickness vs time evolution during the deposition of 290 nm ZnO:Al at 2 mTorr and 150 °C with 0.2 sccm O₂. Comparison between Si/SiO₂ and glass substrates.

with the deposition temperature. On the opposite, since $\alpha_{Si} = (1.000 + 0.0055 T) \times 10^{-6}/K$ (in the same temperature range) is smaller than α_{ZnO} , it is then tensile stress that is induced in case of deposition on Si/SiO₂ substrates. As can be seen in Fig. 9, the level of the thermal stress upon cooling might be as large as to the one of the growth-induced stress, which illustrates the interest of following the internal stress evolution in situ during deposition. Indeed, a final low stress level determined ex situ is not sufficient to ensure a stress-free deposition, since it may result from the cancelation of two large and opposite stress distributions.

Furthermore, we wish to point out an additional subtlety in measuring the stress of a transparent layer with the laser-based MOSS technique. We recall that this technique simply consists in the very precise monitoring into a CCD camera of both the spacings and intensities of a set of coherent laser spots reflecting off a substrate that is free to bend. For non-transparent coatings, only changes in the spot positions are generally considered, which allow monitoring tiny curvature change of the substrate. For transparent coatings, this technique is relatively easy to setup in the case of an opaque substrate such as Si. In that case, the

reflected beam is mainly composed of a beam reflecting off the Si substrate, superimposed on the reflected beam at the outer surface of the TCO. Indeed, even if the TCO is largely transparent, the sudden change of refractive index between the vacuum media ($n_{vac}=1$) and ZnO:Al ($n_{AZO}=1.9$ [23]) causes a substantial amount R of specular reflection under normal incidence, given by

$$R = \frac{(n_1 - n_2)^2}{(n_1 + n_2)^2} \quad (3)$$

This amounts to 10% at the vacuum—ZnO:Al interface and to 20% at the SiO₂—Si interface (the 1% reflection at the ZnO:Al—SiO₂ interface can be neglected here). The laser spots, the precise positions of which are recorded to infer the curvature change according to Eq. (1), are therefore always constituted of the superposition of those two reflected beams. As a result, the intensity of those spots bear some interesting information since the beam reflected at the outer interface can interfere with the one reflected at the Si surface. In fact, when measuring on Si/SiO₂ substrates, the incident laser power is not kept constant but rather adjusted in realtime such that the most intense spot always corresponds to 90% saturation of the CCD camera. The typical evolution of the laser power level required to fulfill that condition is shown in Fig. 10a. This reported evolution is typical for the interference of two beams having the same wavelength but different intensities. Indeed, as the thickness of the ZnO:Al layer is increasing, interferences between those two sets of beams start evolving. In particular, each time the thickness of ZnO:Al corresponds to odd multiples of a quarter of the laser wavelength λ_0 , a destructive interference occurs. At that moment, the laser power has to be brought to its maximum in order to maintain the spot intensity at the pre-set level of 90% saturation. The periodicity of these destructive interferences is simply given by $\lambda_0/(2 \cdot n_{AZO}) = 173$ nm and corresponds to the one observed. Therefore, the additional information carried into the spot intensity or into the laser power is similar to an in situ thickness measurement laser interferometry.

In case of growth of a transparent conducting layer on a transparent glass substrate, the situation is slightly more complex. Indeed, even though according to Eq. (3) there is still a reflection of 4% at the vacuum—glass ($n_{glass}=1.5$) interface before the deposition takes place, there is also a reflection coming from the back side of the glass substrate. However, since the glass substrate is much thicker (400 μ m) than the subsequently deposited layer and thanks to the fact that the two glass sides are not perfectly perpendicular to the beams, the spot array corresponding to the beams reflected off the back side of the substrate can be separated from the one coming off the frontside. In the case of the glass substrates, the laser intensity was not adapted in situ to match a given constant peak intensity but was rather kept constant. In that case, the increase in film thickness can directly be followed from the evolving spot intensity, as shown in Fig. 10b. Once again, the same interference mechanism between the outer reflected beam and the beam reflected at the glass—ZnO:Al interface with the same thickness periodicity was observed. We note that the final thicknesses inferred this way matched extremely well the one measured by cross-sectional SEM when taking the bulk refractive index value $n_{AZO}=1.9$ for the deposit. Only a small discrepancy was observed for the depositions carried at 6 and 10 mTorr where a lower film refractive index value was necessary to conciliate the data. This can be taken indicative for the presence of some porosity at those very large working pressures.

3.3. Internal stress evolution and electro-optical properties

The evolution of the resistivity and the transmittance at a typical visible wavelength (550 nm) is presented in Fig. 11 with respect to

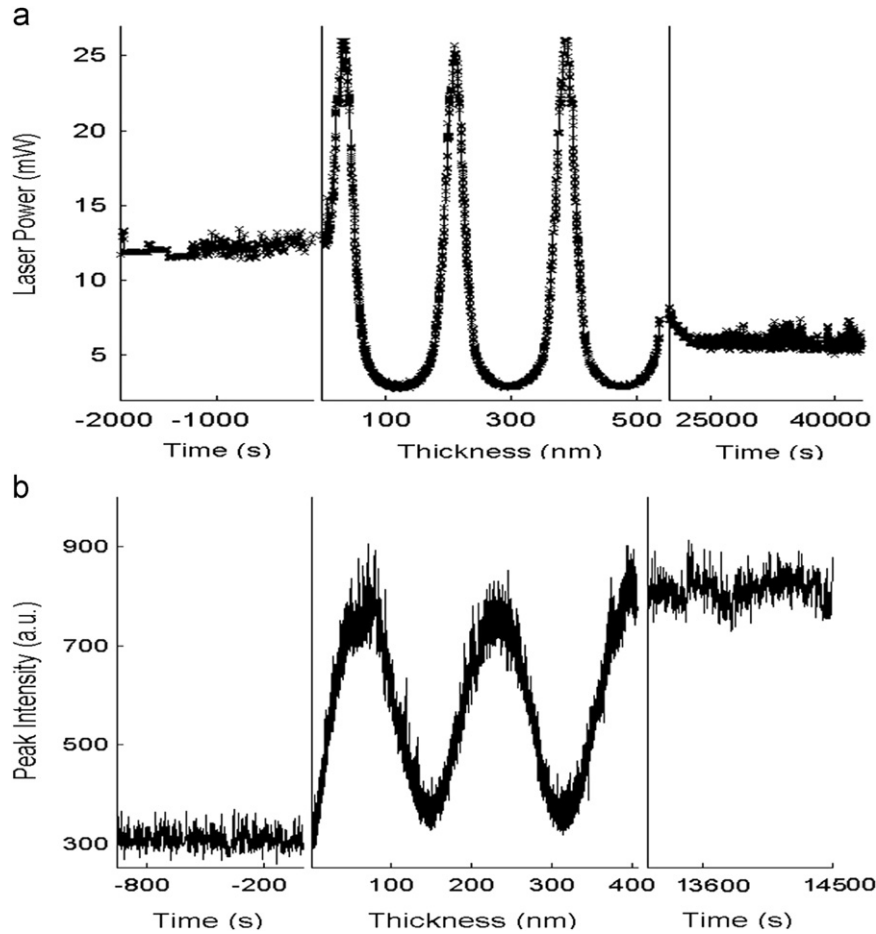


Fig. 10. Evolution before, during and after the deposition of ZnO:Al films at 2 mTorr, 150 °C and 0.2 sccm oxygen flow of: (a) MOSS laser power adjusted in real time in case of Si/SiO₂ substrates such that the brightest spot intensity is kept at 90% of the CCD camera saturation threshold, (b) typical peak intensity variation of each spot recorded by the MOSS CCD camera in case of glass substrates where the laser power is kept constant (4 mW).

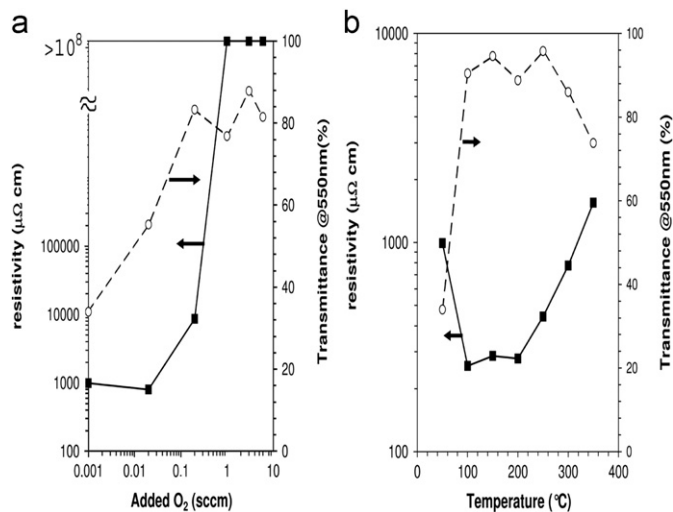


Fig. 11. Resistivity and transmittance at a wavelength of 550 nm for 400 nm thick ZnO:Al films deposited at 2 mTorr on glass substrates with: (a) no heating and varying the oxygen gas flow, or (b) no oxygen gas addition and varying the substrate temperature.

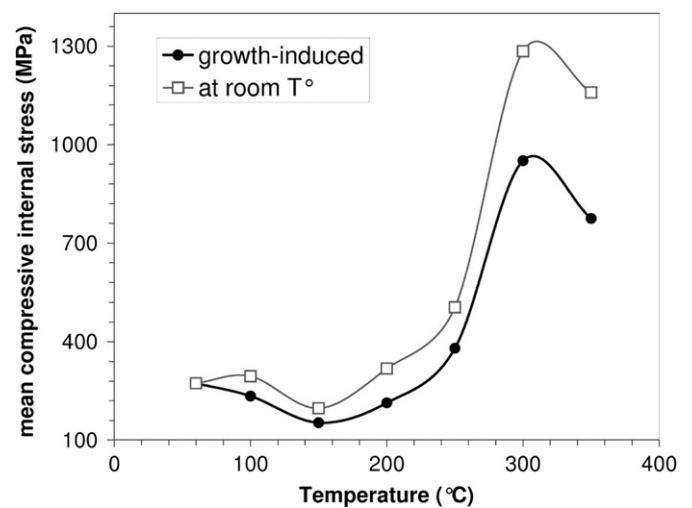


Fig. 12. Growth-induced and room temperature resulting mean internal (compressive) stress level vs. substrate temperature for 400 nm thick ZnO:Al films deposited at 2 mTorr on glass substrate without oxygen gas addition.

the oxygen addition or the substrate temperature. As a compromise between a good electrical conduction and a good optical transparency in the visible, the optimization of those electro-optical functional properties leads us to select a substrate temperature of 150 °C, since it gives roughly the minimum resistivity (Fig. 11b). This minimum of

resistivity also correlates with the minimum growth-induced mean internal stress level as well as with the minimum final mean internal stress level at room temperature (when the thermal stress contribution upon cooling is also included), both inferred from Fig. 7 and illustrated in Fig. 12. A small oxygen addition of 0.2 sccm was also

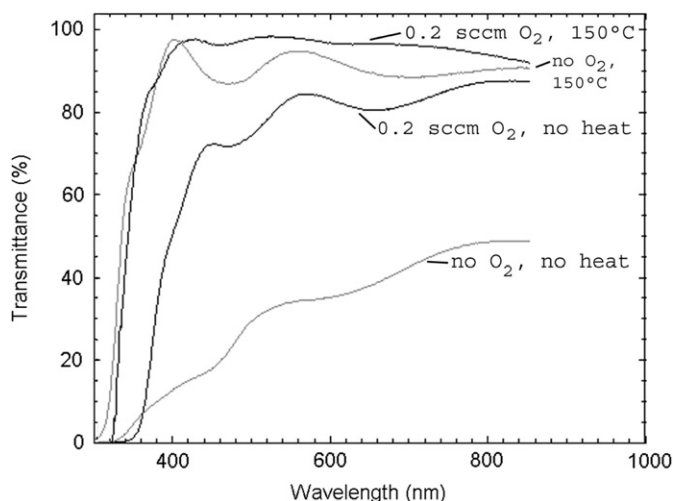


Fig. 13. Transmittance of 400 nm thick ZnO:Al films deposited at 2 mTorr on glass substrates with either no oxygen gas addition or 0.2 sccm oxygen gas flow, as well as with either no substrate heating or 150 °C heating.

selected because of its drastic improvement of the optical transmittance, despite the small resistivity increase. As explained above that amount of oxygen is also the one which induces the largest tensile instantaneous stress. This can be taken in turn to be indicative for the strongest grain “zipping” interaction. For those two optimum deposition parameters, i.e. 0.2 sccm oxygen and 150 °C heating, the internal growth-related stress evolution is dominated by the atomic peening contribution as well as the diffusion along the grain boundaries and presents therefore a compressive overall behavior (Fig. 9). Resulting 400 nm thick ZnO:Al layers in turn typically had a resistivity between 300 and 400 $\mu\Omega$ cm (corresponding to a resistance between 7 and 10 Ω/\square) and a transparency above 90% in the full visible spectra. The full spectral dependence of the transmission is presented in Fig. 13 in case of heating to 150 °C (or not) as well as in case of 0.2 sccm oxygen addition (or not). Since the surface of the deposited ZnO:Al layer is quite smooth, interference fringes are also present [24].

4. Conclusions

In conclusion, the evolution of the internal stress of sputtered ZnO:Al layers measured in situ on opaque or transparent substrates and its dependence on the main deposition parameters have been presented. The main findings of our paper are as follows:

- The fact that the deposit and/or the substrate are transparent is not an issue for the laser-based curvature measurement technique used for monitoring the internal stress evolution. Moreover, while spot position detection allows for in situ monitoring of curvature changes, the spot intensity allows inferring the thickness evolution of the deposited transparent layers.
- Depending on the deposition parameters, ZnO:Al films with either a tensile or a compressive instantaneous internal stress can be obtained.
- The optimum oxygen addition level as well as the optimum substrate temperature in terms of the electro-optical functional properties of the ZnO:Al layers correspond to particular transitions in the measured internal stress evolution.

Monitoring in situ the internal stress evolution therefore not only helps to gain insight in the film growth mechanism but also to determine the best deposition parameters for optimum electro-optical functional properties.

Acknowledgments

This work has been funded by the European and Wallonia Region FEDER grant ECP12020011678F (MINATIS Project). The authors thank I. Sбилle for XRD measurements as well as the clean-room facility WINFAB of UCL for hosting the deposition equipment.

References

- [1] E. Ando, M. Miyazaki, Durability of doped zinc oxide/silver/doped zinc oxide low emissivity coatings in humid environment, *Thin Solid Films* 516 (2008) 4574–4577.
- [2] U. Rau, M. Schmidt, A. Jasenek, G. Hanna, H.W. Schock, Electrical characterization of Cu(In,Ga)Se₂ thin-film solar cells and the role of defects for the device performance, *Solar Energy Materials & Solar Cells* 67 (1999) 137–143.
- [3] M. Berginski, J. Hupkes, M. Schulte, G. Schope, H. Stiebig, B. Rech, M. Wuttig, The effect of front ZnO:Al surface texture and optical transparency on efficient light trapping in silicon thin-film solar cells, *Journal of Applied Physics* 101 (2007) 074903–074911.
- [4] J.-C. Cho, Y.-J. Kim, J.C. Lee, S.-H. Park, K.H. Yoon, Structural and optical properties of textured ZnO:Al films on glass substrates prepared by in-line rf magnetron sputtering, *Solar Energy Materials & Solar Cells* 95 (2011) 190–194.
- [5] H. Windischmann, Intrinsic stress in sputter-deposited thin films, *Critical Reviews in Solid State and Materials Sciences* 17 (1992) 547–596.
- [6] G.C.A.M. Janssen, Stress and strain in polycrystalline thin films, *Thin Solid Films* 515 (2007) 6654–6664.
- [7] R. Koch, Stress in evaporated and sputtered thin films – a comparison, *Surface & Coatings Technology* 204 (2010) 1973–1982.
- [8] A. Asadov, W. Gao, Z. Li, J. Lee, M. Hodgson, Correlation between structural and electrical properties of ZnO thin films, *Thin Solid Films* 476 (2005) 201–205.
- [9] C. Guillen, J. Herrero, High conductivity and transparent ZnO:Al films prepared at low temperature by DC and MF magnetron sputtering, *Thin Solid Films* 515 (2006) 640–643.
- [10] A.I. Ievtushenko, V.A. Karpyna, V.I. Lazorenko, G.V. Lashkarev, V.D. Khranovskyy, V.A. Baturin, O.Y. Karpenko, M.M. Lunika, K.A. Avramenko, V.V. Strelchuk, O.M. Kutsay, High quality ZnO films deposited by radio-frequency magnetron sputtering using layer by layer growth method, *Thin Solid Films* 518 (2010) 4529–4532.
- [11] F. Couzinie-Devy, N. Barreau, J. Kessler, Dependence of ZnO:Al properties on the substrate to target position in RF sputtering, *Thin Solid Films* 516 (2008) 7094–7097.
- [12] X.B. Zhang, Z.L. Pei, J. Gong, C. Sun, Investigation on the electrical properties and inhomogeneous distribution of ZnO:Al thin films prepared by dc magnetron sputtering at low deposition temperature, *Journal of Applied Physics* 101 (2007) 014910–014917.
- [13] J.A. Floro, S.J. Hearne, J.A. Hunter, P. Kotula, E. Chason, S.C. Seel, C.V. Thompson, The dynamic competition between stress generation and relaxation mechanisms during coalescence of Volmer-Weber thin films, *Journal of Applied Physics* 89 (2001) 04886–04892.
- [14] E. Chason, B.W. Sheldon, Monitoring stress in thin films during processing, *Surface Engineering* 19 (2003) 387–391.
- [15] K. Wasa, M. Kitabatake, H. Adachi, *Thin Film Materials Technology: Sputtering of Compound Materials*, W. Andrew Publishing, ISBN: 0-8155-1483-2, 2004, pp. 219–228.
- [16] J.F. Chang, C.C. Shen, M.H. Hon, Growth characteristics and residual stress of RF magnetron sputtered ZnO:Al films, *Ceramics International* 29 (2003) 245–250.
- [17] R.J. Drese, M. Wuttig, Stress evolution during growth in direct-current-sputtered zinc oxide films at various oxygen flows, *Journal of Applied Physics* 98 (2005) 073514–073515.
- [18] J. Hinz, K. Ellmer, In situ measurement of mechanical stress in polycrystalline zinc-oxide thin films prepared by magnetron sputtering, *Journal of Applied Physics* 88 (2000) 02443–02448.
- [19] J.A. Thornton, High rate thick film growth, *Annual Review of Materials Science* 7 (1977) 239–260.
- [20] K. Oura, V.G. Lifshits, A.A. Saranin, A.V. Zotov, M. Katayama, *Surface Science: An Introduction*, Springer, Berlin, 2003 ISBN 3-540-00545-5.
- [21] J.W. Shin, E. Chason, Compressive stress generation in Sn thin films and the role of grain boundary diffusion, *Physical Review Letters* 103 (2009) 056102–056104.
- [22] A.J. Detor, A.M. Hodge, E. Chason, Y. Wang, H. Xu, M. Conyers, A. Nikroo, A. Hamza, Stress and microstructure evolution in thick sputtered films, *Acta Materials* 57 (2009) 2055–2065.
- [23] S. Adachi, *Optical Constants of Crystalline and Amorphous Semiconductors: Numerical Data and Graphical Information*, Kluwer Academic, Boston, 1999.
- [24] R. Swanepoel, Determination of the thickness and optical constants of amorphous silicon, *Journal of Physics E: Scientific Instruments* 16 (1983) 1214–1222.